738 *Biochemistry* **2011,** *50,* 738–751
DOI: 10.1021/bi101777f

BIOCHEMISTRY
including biophysical chemistry & molecular biology
Article

Biochemical Characterization of TAK-593, a Novel VEGFR/PDGFR Inhibitor with a Two-Step Slow Binding Mechanism

Hidehisa Iwata,[‡] Shinichi Imamura,[§] Akira Hori,[§] Mark S. Hixon,[∥] Hiroyuki Kimura,[‡] and Hiroshi Miki*[,‡]

[‡]*Pharmaceutical Research Division, Takeda Pharmaceutical Company Ltd., 2-17-85, Jusohonmachi Yodogawa-ku, Osaka 532-8686, Japan,* [§]*Pharmaceutical Research Division, Takeda Pharmaceutical Company Ltd., 10, Wadai, Tsukuba, Ibaraki 300-4293, Japan, and* [∥]*Takeda San Diego Inc., 10410 Science Center Drive, San Diego, California 92121, United States*

Received November 5, 2010; Revised Manuscript Received December 14, 2010

ABSTRACT: Inhibition of tumor angiogenesis leads to a lack of oxygen and nutrients in the tumor and therefore has become a standards of care for many solid tumor therapies. Dual inhibition of vascular endothelial growth factor receptor (VEGFR) and platelet-derived growth factor receptor (PDGFR) protein kinase activities is a popular strategy for targeting tumor angiogenesis. We discovered that TAK-593, a novel imidazo[1,2-*b*]pyridazine derivative, potently inhibits tyrosine kinases from the VEGFR and PDGFR families. TAK-593 was highly selective for these families, with an $IC_{50} > 1\ \mu M$ when tested against more than 200 protein and lipid kinases. TAK-593 displayed competitive inhibition versus ATP. In addition, TAK-593 inhibited VEGFR2 and PDGFRβ in a time-dependent manner, classifying it as a type II kinase inhibitor. Analysis of enzyme−inhibitor preincubation experiments revealed that the binding of TAK-593 to VEGFR2 and PDGFRβ occurs via a two-step slow binding mechanism. Dissociation of TAK-593 from VEGFR2 was extremely slow ($t_{1/2} > 17$ h), and the affinity of TAK-593 at equilibrium (K_i*) was less than 25 pM. Ligand displacement analysis with a fluorescent tracer confirmed the slow dissociation of TAK-593. The dissociation rate constants were in good agreement between the activity and ligand displacement data, and both analyses supported slow dissociation of TAK-593. The long residence time of TAK-593 may achieve an extended pharmacodynamic effect on VEGFR2 and PDGFRβ kinases in vivo that differs substantially from its observed pharmacokinetic profile.

Angiogenesis, i.e., the development of new blood vessels to supply oxygen and nutrients, plays a pivotal role in the growth of solid tumors (*1*). Vascular endothelial growth factors (VEGFs) are key stimulators of tumor angiogenesis that promote events such as endothelial cell proliferation (*2*). VEGFs are soluble dimerized glycoproteins with molecular masses of approximately 40 kDa. In mammals, five members of the VEGF family have been identified (VEGFA, VEGFB, VEGFC, VEGFD, and placental growth factor) (*3*). There are three vascular endothelial growth factor receptors (VEGFRs) known as VEGFR1 (Flt1), VEGFR2 (KDR/Flk1), and VEGFR3 (Flt4). They are members of the receptor tyrosine kinase (RTK) family belonging to the same subclass as the receptors for platelet-derived growth factors (PDGFs) and fibroblast growth factors (FGFs). Each VEGF receptor forms a homodimer or heterodimer (VEGFR1/VEGFR2 and VEGFR2/VEGFR3) upon binding with the appropriate VEGF isoform. VEGFR2 is one of the cell surface-expressed tyrosine kinase receptors that binds specifically with VEGF and transduces its signals. Recently, it was reported that VEGF pathway inhibitors displayed invasive tumor growth in some cases (*4*). However, VEGF signaling blockade is effective, and several low molecular weight inhibitors of VEGFR2 kinase activity have progressed through preclinical and clinical development and some have even been marketed (*5*−*7*).

The platelet-derived growth factor (PDGF) family also plays an important role in tumor angiogenesis through the receptors PDGFRα and PDGFRβ. During angiogenesis, PDGFs produced by endothelial cells and tumor cells activate smooth muscle cell-like pericytes to stabilize newly formed blood vessels (*8*). Along with VEGFRs and PDGFRs, c-Kit[1] receptor tyrosine kinase is a member of the PDGFR and FGFR superfamily, and its signaling is believed to play a role in tumorigenesis (*9*). Recent studies have suggested that therapy with Sunitinib (Figure1) (Sutent, a low molecular weight inhibitor of VEGFR2 kinase, PDGFRβ kinase, and c-Kit kinase) or Sorafenib (Figure1) (Nexavar, a low molecular weight inhibitor of VEGFR2 kinase, B-Raf kinase, and PDGFRβ kinase) has a profound antiangiogenic effect in vivo (*10*), as well as antitumor activity against gastrointestinal stromal tumors (GISTs) and renal cell carcinoma (RCC) (*11*).

The activity of RTKs is tightly repressed by a cis inhibition/transactivation mechanism until the receptor is stimulated by its corresponding ligand (*12*).

The equilibrium between inactive and active conformations of unphosphorylated RTK in solution shifts toward the active conformation upon ligand binding (*13*). In the unstimulated state, the Asp-Phe-Gly (DFG) motif at the beginning of the activation loop of the RTK protrudes and interferes with substrate access to the active site (*14*). This inactive conformation is called the DFG-out conformation. After an RTK is stimulated by its ligand, it forms

*Corresponding author. Tel: +81-6-6308-9046. Fax: +81-6-6308-9017. E-mail: miki_hiroshi@takeda.co.jp.

[1]Abbreviations: ATP, adenosine 5′-triphosphate; DMSO, dimethyl sulfoxide; DTT, DL-dithiothreitol; EDTA, ethylenediamine-*N*,*N*,*N*′,*N*′-tetraacetic acid; $MgCl_2$, magnesium chloride; $MnCl_2$, manganese chloride; Tris, tris(hydroxymethyl)aminomethane; Tween-20, polyoxyethylene(20)sorbitan monolaurate; IC_{50}, inhibitor concentration producing 50% inhibition; c-Kit, v-kit Hardy−Zuckerman 4 feline sarcoma viral oncogene homologue; EGFR, epidermal growth factor receptor; HER2, human epidermal growth factor receptor 2; HER4, human epidermal growth factor receptor 4; FGFR, fibroblast growth factor receptor; Src, v-src avian sarcoma viral oncogene homologue (Schmidt−Ruppin A-2) 1; B-Raf, v-raf murine sarcoma viral oncogene homologue B1.

 Published on Web 12/23/2010 © 2010 American Chemical Society

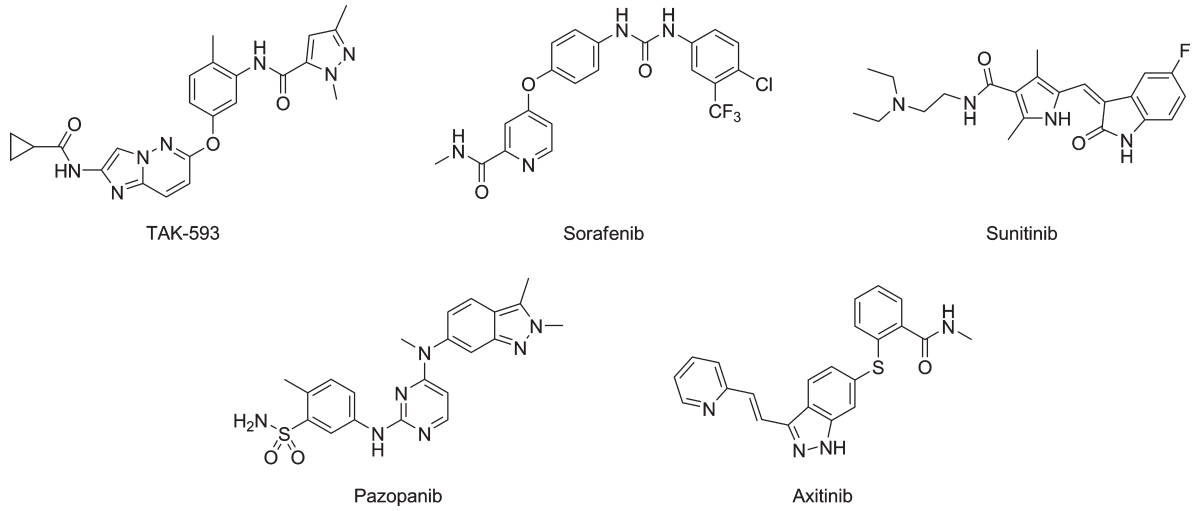

FIGURE 1: Chemical structures of TAK-593 and other VEGFR2 inhibitors.

an oligomer that triggers autophosphorylation of its tyrosine residues, including the residues required for enzyme activation that are located in the activation loop of the kinase domain. Autophosphorylation of the activation loop shifts the equilibrium toward the active conformation and shifts the DFG motif to the DFG-in conformation, facilitating substrate access to the active site. When designing kinase inhibitors to target receptor protein kinases, it is important to determine the ability of a putative inhibitor to inhibit the inactive form of the enzyme (*15*). The majority of kinase inhibitors target the activated form of the enzyme with a DFG-in conformation of its activation loop, and these are categorized as type I inhibitors. In contrast, some kinase inhibitors (so-called type II inhibitors) bind with the canonical ATP-binding site of the kinase domain and induce the enzyme with an inactive conformation (DFG-out) of its activation loop or a C-helix-out conformation. The first known example was STI-571 (imatinib mesylate/Gleevec), with Abelson tyrosine kinase (Abl) adopting the DFG-out conformation (*16*, *17*). Type II inhibitors have some advantages over type I ATP site inhibitors, including slower dissociation (*18*, *19*). For example, Lapatinib (Tykerb), a potent HER2/EGFR dual inhibitor, has been shown to mostly bind with the inactive conformation of EGFR (a C-helix-out conformation) through various biochemical and structure biological studies (*20*). This unique binding mode enables Lapatinib to bind tightly with EGFR, and as a result Lapatinib dissociates very slowly from the enzyme. In other words, the long residence time of Lapatinib on the receptor is thought to result from its unique mode of binding. Moreover, the long residence time of Lapatinib may account for its high potency in tumor cell proliferation assays (*21*). On the other hand, Gefitinib (Iressa) and Erlotinib (Tarceva) are potent selective EGFR inhibitors that exclusively bind with the active conformation of EGFR and dissociate rapidly. With respect to VEGFR2 kinase inhibitors, among approved inhibitors Sunitinib is a type I inhibitor; on the other hand Sorafenib and Pazopanib (Votrient) (Figure 1) are type II inhibitors. Additionally, there is a type II inhibitor, Axitinib (Figure 1), which is reported to be highly potent against nonphosphorylated VEGFR2 and to have a long residence time with the targeted enzyme (*22*) and reported to be in clinical study for various solid tumors (*23*).

Inhibitors with a long residence time usually also display slow binding inhibition in enzymatic analyses(*24*). There are two common mechanisms that describe slow binding inhibition (Schemes 1 and 2).

Scheme 1: One-Step Slow Binding Mechanism

$$E \underset{k_2}{\overset{k_1[I]}{\rightleftharpoons}} EI$$

Scheme 2: Two-Step Slow Binding Mechanism

$$E \underset{k_2}{\overset{k_1[I]}{\rightleftharpoons}} EI \underset{k_4}{\overset{k_3}{\rightleftharpoons}} E^*I$$

Scheme 1 represents a one-step binding mechanism with a slow association rate constant (k_1) and an even slower dissociation rate constant (k_2), leading to the slow onset of inhibition. Inhibition of angiotensin-converting enzyme by captopril or enalapril is consistent with this one-step binding inhibition mechanism (*25*). On the other hand, the two-step binding mechanism illustrated in Scheme 2 involves two steps to reach a final equilibrium of inhibition. The initial enzyme-inhibitor (EI) complex forms rapidly and then slowly proceeds to a more stable enzyme–inhibitor complex (EI*). Inhibition of dipeptidyl peptidase 4 by vildagliptin (*26*) and inhibition of HIV-1 integrase by L-870,810 (*27*) are processes that are consistent with two-step binding inhibition.

As a result of lead compound optimization to obtain an orally active low molecular weight compound that potently and selectively inhibits VEGFR and PDGFR, we identified TAK-593 (Figure 1) as a novel potent tumor angiogenesis inhibitor. Here, we describe the kinase selectivity and inhibition mechanism of TAK-593 evaluated by enzymatic activity and ligand displacement analyses of VEGFR2 and PDGFRβ. In these analyses, TAK-593 displayed an extremely slow two-step binding mechanism for these two kinases (Scheme 2), which is sometimes ambiguously referred to as pseudoirreversible inhibition (*28*). This mechanism may contribute to the prolonged action of TAK-593 against VEGFR2 and PDGFRβ kinases in both clinical and preclinical studies.

MATERIALS AND METHODS

Chemicals. TAK-593 (*N*-[5-({2-[(cyclopropylcarbonyl)amino]-imidazo[1,2-*b*]pyridazin-6-yl}oxy)-2-methylphenyl]-1,3-dimethyl-1*H*-pyrazole-5-carboxamide) was synthesized by Takeda Pharmaceutical Co. Ltd. (Osaka, Japan). Sorafenib (Nexavar; Bayer, Germany) and Sunitinib (Sutent; Pfizer, USA) were obtained from commercial sources.

Reagents. FLAG M2 affinity gel, ATP, DTT, and poly-Glu-Tyr (4:1) were purchased from Sigma-Aldrich (MO, USA). An amplified luminescent proximity homogeneous assay (AlphaScreen) phosphotyrosine (P-Tyr 100) assay kit and AlphaScreen phosphotyrosine (PT66) assay kit were purchased from PerkinElmer (MA, USA). [γ-^{32}P]ATP was obtained from GE Healthcare (WI, USA). Biotinylated poly-Glu-Tyr (4:1) was purchased from Cisbio (France). 5 × kinase buffer A, Eu-anti-His-tag antibody, and kinase tracer 236 for the LanthaScreen Eu kinase binding assay were obtained from Invitrogen (CA, USA). Recombinant human cytoplasmic domain of VEGFR1 (Flt-1) (783−1338) with N-terminal 6 × His tag, VEGFR2 (FLK-1/KDR) (790−1356) with N-terminal 6 × His tag, VEGFR3 (Flt4) (800−1363) with N-terminal GST tag, PDGFRα (550−1089) with N-terminal 6 × His tag, PDGFRβ (550−1106) with N-terminal 6 × His tag, c-Kit (544−976) with N-terminal GST tag, and recombinant human catalytic domain of HER4 (706−991) with N-terminal 6 × His tag were purchased from Upstate (now part of Millipore, MA, USA). Each kinase was expressed by baculovirus in Sf21 insect cells. The amino acid sequences of VEGFR2 and PDGFRβ are shown in Supporting Information Figure S1.

Preparation of Recombinant Kinases. For HER2 kinase, the cytoplasmic domain (amino acids 676−1255) of human HER2 was expressed as an N-terminal peptide (DYKDDDD) tagged protein in a baculovirus expression system. The expressed HER2 kinase protein was purified with anti-FLAG M2 affinity gel. For EGFR kinase, the cytoplasmic domain (amino acids 669−1210) of human EGFR was expressed as an N-terminal peptide (DYKDDDD) tagged protein using a baculovirus expression system. The expressed EGFR kinase protein was purified by using anti-FLAG M2 affinity gel.

Inhibitory Activity against VEGFRs and PDGFRs. VEGFR and PDGFR kinase activity was determined with an anti-phosphotyrosine antibody and was quantified through the AlphaScreen system (PerkinElmer, USA). In all experiments, the ATP concentration was held at apparent K_m (K_m^{app}). For VEGFR2, enzyme reactions were performed in 50 mM Tris-HCl (pH 7.5), 5 mM $MnCl_2$, 5 mM $MgCl_2$, 0.01% Tween-20, and 2 mM DTT, containing 10 μM ATP at K_m^{app}, 0.1 μg/mL biotinylated poly-Glu-Tyr (4:1), and 0.3 nM recombinant cytoplasmic domain of VEGFR2 (Milliopre). Prior to the catalytic initiation with ATP, the compound and enzyme were incubated for 5 min at ambient temperature. After 10 min of enzyme reaction, the reaction was quenched by addition of 25 μL of 100 mM EDTA, 10 μg/mL AlphaScreen streptavidin donor beads, and 10 μg/mL P-Tyr-100 coated acceptor beads in 62.5 mM HEPES (pH 7.4) with 250 mM NaCl and 0.1% BSA. Plates were incubated in the dark overnight and then read on an EnVision 2102 multilabel reader (PerkinElmer). For PDGFRβ, the enzyme assay was performed as described above for 30 min with 0.8 nM recombinant cytoplasmic domain of PDGFRβ (Millipore) and 10 μg/mL PT66 coated donor beads. For other kinases, the reaction conditions are described in Supporting Information Table S1.

Wells containing the substrate and the enzyme without the compound were used as the total reaction control. Wells containing biotinylated poly-Glu-Tyr (4:1) and the enzyme without ATP were used as the basal control. The concentration of TAK-593 that achieved 50% inhibition of the kinase activities of VEGFR1, VEGFR2, VEGFR3, PDGFRα, PDGFRβ, and c-Kit (IC_{50} values) was analyzed using GraphPad Prism version 5.01 (GraphPad Software, CA, USA). Sigmoidal dose−response (variable slope) curves were fitted using nonlinear regression analysis, with the top and bottom of the curve being constrained at 100 and 0, respectively.

Kinetic Mechanism of Inhibition for ATP. To investigate the kinetic mechanism of ATP inhibition by TAK-593 during inhibition of VEGFR2 and PDGFRβ, assays were performed at various ATP concentrations without preincubation of the enzyme and TAK-593 using the AlphaScreen procedure as described above. Obtained results were fitted to a competitive kinetic mechanism of inhibition in GraphPad Prism 5.01.

Kinase Selectivity Panel Experiments. The kinase activities of HER2, EGFR, and HER4 were determined by filtration assays using radiolabeled [γ-^{32}P]ATP. Enzyme reactions were performed in 50 mM Tris-HCl (pH 7.5), 5 mM $MnCl_2$, 0.01% Tween-20, and 2 mM DTT containing 0.9 μCi of [γ-^{32}P]ATP per reaction, as well as 50 μM ATP, 5 μg/mL poly-Glu-Tyr (4:1), 0.1% DMSO, and a suitable concentration of recombinant kinase for the assay (Supporting Information Table S1). The inhibitory activity of TAK-593 against Aurora-A, CDK1/cyclinB, CDK2/cyclinA, CDK2/cyclinE, c-Met, FAK, FGFR1, GSK3β, IGF-1R, IR, MEK1, PKCθ, Src(1−530), and Tie2 was measured by using the IC_{50} Profiler Express selectivity screening service (Millipore, U.K.). The inhibitory activity of TAK-593 against B-Raf was measured by using QuickScout custom profiling service (Carna Biosciences, Japan).

The inhibitory activity of TAK-593 (1 μM) against 265 human kinases was determined by using the KinaseProfiler selectivity screening service (Millipore, U.K.). Screening was performed with the ATP concentration set at K_m^{app} for each enzyme. Then we performed further assays at various concentrations of TAK-593 for determination of the IC_{50} against 21 kinases: Abl, Abl (H396P), Abl (M351T), Abl (Q252H), c-Kit (D816H), ALK, c-Kit (V560G), c-Kit (V654A), FGFR2, FGFR2 (N549H), Fgr, Fms, Fms (Y969C), Hck, Lyn, PAK4, PDGFRα (D842 V), PDGFRα (V561D), Ret, Ret (V804M), and Yes.

Time-Dependent Inhibition of VEGFR2 and PDGFRβ. In order to examine the time dependence of TAK-593 binding, assays were performed with various preincubation times of the enzyme and TAK-593 with the ATP concentration set at K_m^{app} using the AlphaScreen procedure as described above. IC_{50} values were calculated by logistic regression analysis (GraphPad Prism 5). The fractional activities obtained at each preincubation time were fitted to eq 1 (*29*):

$$Y = v_i \exp(-k_{obs}t) \quad (1)$$

where Y is fractional activity, v_i is steady-state velocity without preincubation, and t is preincubation time.

The obtained k_{obs} values were then plotted as a function of the inhibitor concentration. If the slope of k_{obs} vs [inhibitor] was linear, the binding mechanism was considered to be one-step binding inhibition and was fitted to eq 2:

$$k_{obs} = k_1[I] + k_2 \quad (2)$$

Alternatively, if the plot was hyperbolic, indicating rate saturation with respect to inhibitor concentration, then binding was assumed to be a two-step process and k_{obs} should obey eq 3:

$$k_{obs} = k_4 + k_3[I]/(K_i^{app} + [I]) \quad (3)$$

K_i^{app} can be converted to the K_i value by the Cheng and Prusoff equation (*30*). With a two-step binding mechanism, the true affinity of the inhibitor (K_i*) is defined by eq 4:

$$K_i* = k_4K_i/(k_3 + k_4) \quad (4)$$

When K_i is significantly higher than K_i*, eq 3 is reduced to the linear form shown as eq 5:

$$k_{obs} = k_4 + (k_4/K_i{*}^{app})[I] \quad (5)$$

The dissociation half-life ($t_{1/2}$) was calculated with eq 6:

$$t_{1/2} = 0.693/k_4 \quad (6)$$

Equations 2−6 are described in Copeland (*31*).

Ligand Displacement Analysis with the LanthaScreen Eu Kinase Binding Assay. The binding assay was performed in 1× kinase buffer A (Invitrogen) containing 2 mM DTT, 50 nM (K_D value) kinase tracer 236 (Invitrogen), 3 nM Eu-anti-His-tag antibody (Invitrogen), various concentrations of the inhibitor, and 3 nM VEGFR2 (Millipore). At first, the enzyme, Eu-labeled antibody, and kinase tracer 236 were incubated for 60 min at ambient temperature to obtain the maximal LanthaScreen time resolved-fluorescence resonance energy transfer (TR-FRET) signal. Next, various concentrations of the inhibitor were added, and the reduction of TR-FRET signal kinetics was monitored continuously by use of an EnVision 2102 multilabel reader. For PDGFRβ, the binding assay was performed as described above with 100 nM (K_D value) kinase tracer 236, 10 nM Eu-anti-His-tag antibody, and 10 nM PDGFRβ (Millipore). To evaluate $k_{on}{}^{app}$ and $k_{off}{}^{app}$ of the inhibitors, the kinetics of the reduction of the TR-FRET signal ratio (emission at 665 nm/emission at 615 nm) at various inhibitor concentrations were fitted to eq 7 (monophase exponential decay fitting in GraphPad Prism 5.01):

$$Y = (Y_0 - \text{plateau})\exp(-k_{obs}t) + \text{plateau} \quad (7)$$

where Y is the TR-FRET signal ratio, Y_0 is the TR-FRET signal ratio of the reaction when $t = 0$, plateau is the TR-FRET signal ratio of the reaction when $t = \infty$, and k_{obs} is the rate constant for inhibitor binding.

In order to determine rate constants and dissociation half-life, we used eqs 4−6 in the same manner for enzymatic activity-based time-dependent analysis.

Determination of the Dissociation Rate Constant by the Activity-Based Rapid Large Dilution Method. To determine the dissociation rate constant (k_{off}) of the inhibitor, enzyme−inhibitor dilution assays were performed. This assay was based on the determination of k_{off} through the kinetics of the recovery of kinase activity after rapid dilution of the enzyme−inhibitor complex (*31*). Recovery of enzyme activity from a preformed enzyme−inhibitor complex was measured by use of the AlphaScreen system (PerkinElmer, USA). The enzyme (at a 100-fold higher concentration than the final reaction condition) and the inhibitor (at a 10-fold higher concentration than its IC_{50} value) were incubated together in reaction buffer for 60 min at ambient temperature to achieve equilibrium for the enzyme−inhibitor complex. Then the complex was diluted 1:100 in reaction buffer containing 1 mM ATP and 0.1 μg/mL biotinylated poly-Glu-Tyr (4:1) to initiate the kinase reaction. The kinetics of the recovery of kinase activity after rapid dilution were fitted to eq 8 (*32*).

Under the above conditions, k_{obs} represents k_{off} of the enzyme−inhibitor complex, and the dissociation half-life ($t_{1/2}$) was calculated with eq 6 after replacing k_4 by k_{obs}:

$$P = v_s t + [(v_i - v_s)/k_{obs}][1 - \exp(-k_{obs}t)] + P_0 \quad (8)$$

where P is the product of kinase reaction (CPS), P_0 is the background signal of the reaction when $t = 0$, v_i is the initial velocity, v_s is the steady-state velocity, and k_{obs} is the rate constant for inhibition.

Determination of the Dissociation Rate Constant Using the LanthaScreen Eu Kinase Binding Assay. To determine the dissociation rate constant of the inhibitor, a ligand displacement based enzyme−inhibitor dilution assay was performed. This assay involved determination of k_{off} through the kinetics of recovery of the tracer binding signal after rapid dilution of the enzyme−inhibitor complex. Recovery of the tracer binding signal from a preformed enzyme−inhibitor complex was measured by using the LanthaScreen Eu kinase binding assay. The enzyme (at a 100-fold higher concentration than the binding assay conditions) and the inhibitor (at a 10-fold higher concentration than the IC_{50} value) were incubated together in 1 × kinase buffer A containing 2 mM DTT for 60 min at ambient temperature to form the enzyme−inhibitor complex. Then the complex was diluted 1:100 in 1 × kinase buffer A containing 2 mM DTT and 3 nM Eu-anti-His-tag antibody (Invitrogen) to initiate displacement of the inhibitor by an excess of kinase tracer 236. The kinetics of the recovery of tracer binding activity after rapid dilution were normalized as a percentage of tracer bound enzyme (100%; no inhibitor control, 0% no inhibitor and no enzyme control) and fitted to eq 9.

Under these conditions, k_{obs} represents k_{off} of the enzyme−inhibitor complex, and the dissociation half-life was calculated with eq 6, replacing k_4 by k_{obs} in the same manner as for enzymatic activity based rapid dilution analysis.

$$Y = 100 - \text{span}(1 - \exp(-k_{obs}t)) \quad (9)$$

where k_{obs} is the rate constant for inhibition and span is the Y value when $t = \infty$.

RESULTS

TAK-593 Is a Highly Selective, ATP-Competitive VEGFR/PDGFR Inhibitor. TAK-593 is an imidazo[1,2-*b*]pyridazine-based compound (Figure 1). It was shown to potently inhibit the kinase activity of VEGFR1, VEGFR2, VEGFR3, PDGFRα, PDGFRβ, and c-Kit with IC_{50} values of 3.2, 0.95, 1.1, 4.3, 13, and 100 nM, respectively (Table 1 and Supporting Information Figure S2). To determine the inhibitory mechanism toward the substrate ATP, inhibitory assays were performed at various concentrations of ATP without preincubation of the enzyme and the inhibitor. As shown in Figure 2, the apparent value of K_m increased with increasing TAK-593 concentration. These results are consistent with an ATP competitive mechanism for TAK-593. To confirm the kinase selectivity of TAK-593 against cancer-related or well-known kinases, we performed a concentration−response inhibition assay against 17 kinases. Against this limited survey TAK-593 only inhibited FGFR1, Src, and B-Raf with IC_{50} of 350, 5900, and 8400 nM, respectively. Broadening our examination of TAK-593 kinase selectivity, we conducted selectivity assays in the presence of TAK-593 at 1 μM against over 260 human recombinant protein/lipid kinases, including protein kinases with known drug resistance or constitutive active mutations (Supporting Information Table S2). After the single concentration TAK-593 selectivity assay, IC_{50} values were determined for 21 kinases that were observed to be sensitive to TAK-593. The criterion for determination of the IC_{50} value was more than 50% inhibition at 1 μM. We performed concentration−response inhibition assays for a total of 45 kinases summarized in Table 1. TAK-593 potently inhibited (IC_{50} = 10 nM) Fms, which resides within the PDGFR and FGFR superfamily. TAK-593 also inhibited (IC_{50} = 18 nM) Ret, which is closely related to VEGFR

Table 1: Inhibitory Activity of TAK-593 against 45 Kinases

kinase	IC_{50} (nM)	kinase	IC_{50} (nM)
VEGFR1[a]	3.2	Aurora-A	>10000
VEGFR2[a]	0.95	B-Raf[c]	8400
VEGFR3[a]	1.1	CDK1/cyclinB	>10000
PDGFRα[a]	4.3	CDK2/cyclinA	>10000
PDGFRα (D842 V)	35	CDK2/cyclinE	>10000
PDGFRα (V561D)	1	GSK3β	>10000
PDGFRβ[a]	13	MEK1	>10000
c-Kit[a]	100	PAK4	>10000
c-Kit (D816H)	86	PKCθ	>10000
c-Kit (V560G)	3	ALK	>10000
c-Kit (V654A)	61	c-Met	>10000
FGFR1	350	EGFR[b]	>10000
FGFR2	250	FAK	>10000
FGFR2 (N549H)	27	HER2[b]	>10000
Fgr	700	HER4[b]	>10000
Fms	10	IGF-1R	>10000
Fms (Y969C)	35	IR	>10000
Hck	670	Tie2	>10000
Lyn	270		
Ret	18		
Ret (V804M)	1400		
Src	5900		
Yes	160		
Abl	110		
Abl(H396P)	120		
Abl (M351T)	21		
Abl (Q252H)	140		

[a]These IC_{50} determinations were performed by the AlphaScreen assay. [b]These IC_{50} determinations were performed by the radiometric assay. [c]IC_{50} determination for B-Raf was performed using the QuickScout custom-profiling service (Carna Bioscience). The other IC_{50} determinations were performed using KinaseProfiler IC_{50} Express (Millipore).

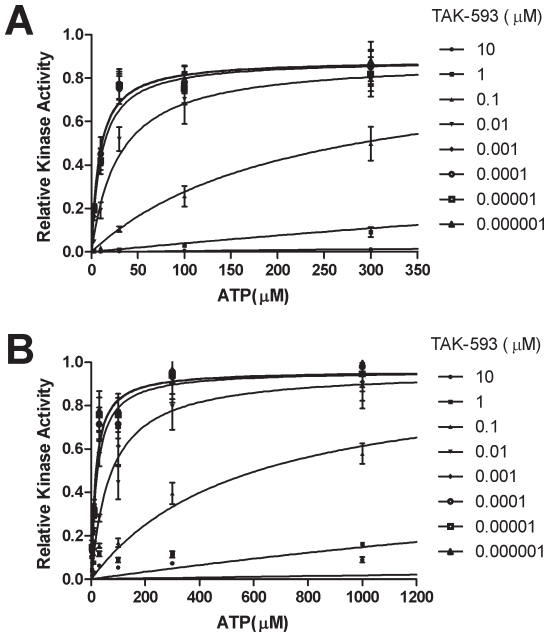

FIGURE 2: Mechanism of inhibition of TAK-593 for VEGFR2 (A) and PDGFRβ (B) with respect to ATP. All experiments were performed in quadruplicate by the AlphaScreen method.

in the kinome, a human kinase dendrogram (*33*). Other than PDGFR and the FGFR superfamily, TAK-593 inhibited Abl and members of the Src kinase family such as Src, Fgr, Lyn, Hck, and Yes with IC_{50} values ranging from 110 to 5900 nM. Surprisingly, TAK-593 did not inhibit any of the Ser/Thr kinases in the assay panel, except for B-Raf with an IC_{50} value of 8400 nM. Thus, we conclude that TAK-593 is a potent, ATP-competitive VEGFR/PDGFR inhibitor with a highly restricted inhibitory spectrum for the human kinome.

Slow Binding Inhibition of VEGFR2 and PDGFRβ by TAK-593. There are recent reports of kinase inhibitors displaying time-dependent inhibition (*19*, *34*). To investigate whether TAK-593 is a slow binding inhibitor of VEGFR2 and PDGFRβ, kinase assays for VEGFR2 and PDGFRβ were performed after varied preincubations the enzyme with TAK-593 (Figure 3A,D). For both enzymes, the IC_{50} values decreased as a function of increasing preincubation time. TAK-593 inhibited VEGFR2 with an IC_{50} of 4.0 nM in the absence of preincubation. On the other hand, after preincubation for 120 min at ambient temperature, TAK-593 inhibited VEGFR2 with an IC_{50} of 36 pM. Thus, at equilibrium, TAK-593 displayed a 111-fold increase of potency over its initial binding complex (Table 2). Likewise, TAK-593 revealed a 6.5-fold increase of potency after preincubation with PDGFRβ (Table 2). By the same method, we evaluated two clinically available multikinase inhibitors, Sorafenib and Sunitinib (Figure 1), to assess time-dependent binding. Like TAK-593, Sorafenib inhibited VEGFR2 and PDGFRβ in a time-dependent manner (Figure 3B,E and Table 2). On the other hand, the inhibition of VEGFR2 and PDGFRβ by Sunitinib essentially occurred via a rapid equilibrium binding mechanism (Figure 3C,F and Table 2). Based on the kinetics of binding to the targets VEGFR2 and PDGFRβ, TAK-593 was mechanistically closer to Sorafenib than to Sunitinib.

Using data from the preincubation experiments, fractional activity was plotted as a function of preincubation time, and eq 1 was employed to obtain k_{obs} values for VEGFR2 and PDGFRβ (Figures 4A−C and 6A−C, respectively). Next, the k_{obs} values were plotted as a function of the TAK-593 concentration (Figures 4D and 6D, respectively). With a one-step binding mechanism (Scheme 1) or a two-step binding mechanism (Scheme 2), there should be linear (*35*) or hyperbolic dependence (*36*) of k_{obs} on the inhibitor concentration, respectively. The hyperbolic dependence displayed in Figures 4D and 6D is consistent with a two-step binding mechanism of TAK-593 for VEGFR2 and PDGFRβ. Nonlinear least-squares fitting of eq 3 to k_{obs} versus inhibitor concentration yielded the microscopic rate constants k_3 and k_4. At a saturating concentration of inhibitor, k_{obs} is equal to $k_3 + k_4$, but since the value of k_4 is negligible (as judged from the near zero *y*-intercept in Figure 4D), we may make the approximation of $k_3 + k_4 \approx k_3 = 1.0 \times 10^{-2}$ s^{-1} for binding to VEGFR2. From the above analysis and correction for the substrate concentration by the Cheng and Prusoff equation (*30*), a K_i of 3.2 nM was obtained. To determine the dissociation rate constant (k_4) for VEGFR2 and PDGFRβ, we performed additional preincubation experiments at much lower inhibitor concentrations than K_i^{app} (Figure 5 and Supporting Information Figure S3, respectively). Under such low inhibitor conditions, eq 3 reduces to the linear form (eq 5) with a *y*-intercept equal to k_4. As seen in Figure 5A−C, k_4 for TAK-593 was determined to be 7.8×10^{-5} s^{-1} (Table 3). From the microscopic rate constants and eq 4, we obtained the true affinity (K_i*) of TAK-593 for VEGFR2 as ~25 pM. The calculated K_i and K_i* values were in good agreement with the activity-based IC_{50} values obtained with and without enzyme−inhibitor preincubation for 120 min. In this situation, k_4 is the rate-limiting step for dissociation of TAK-593 from the enzyme, and the dissociation half-life ($t_{1/2}$) of TAK-593 and VEGFR2 was calculated to be approximately 150 min. In the

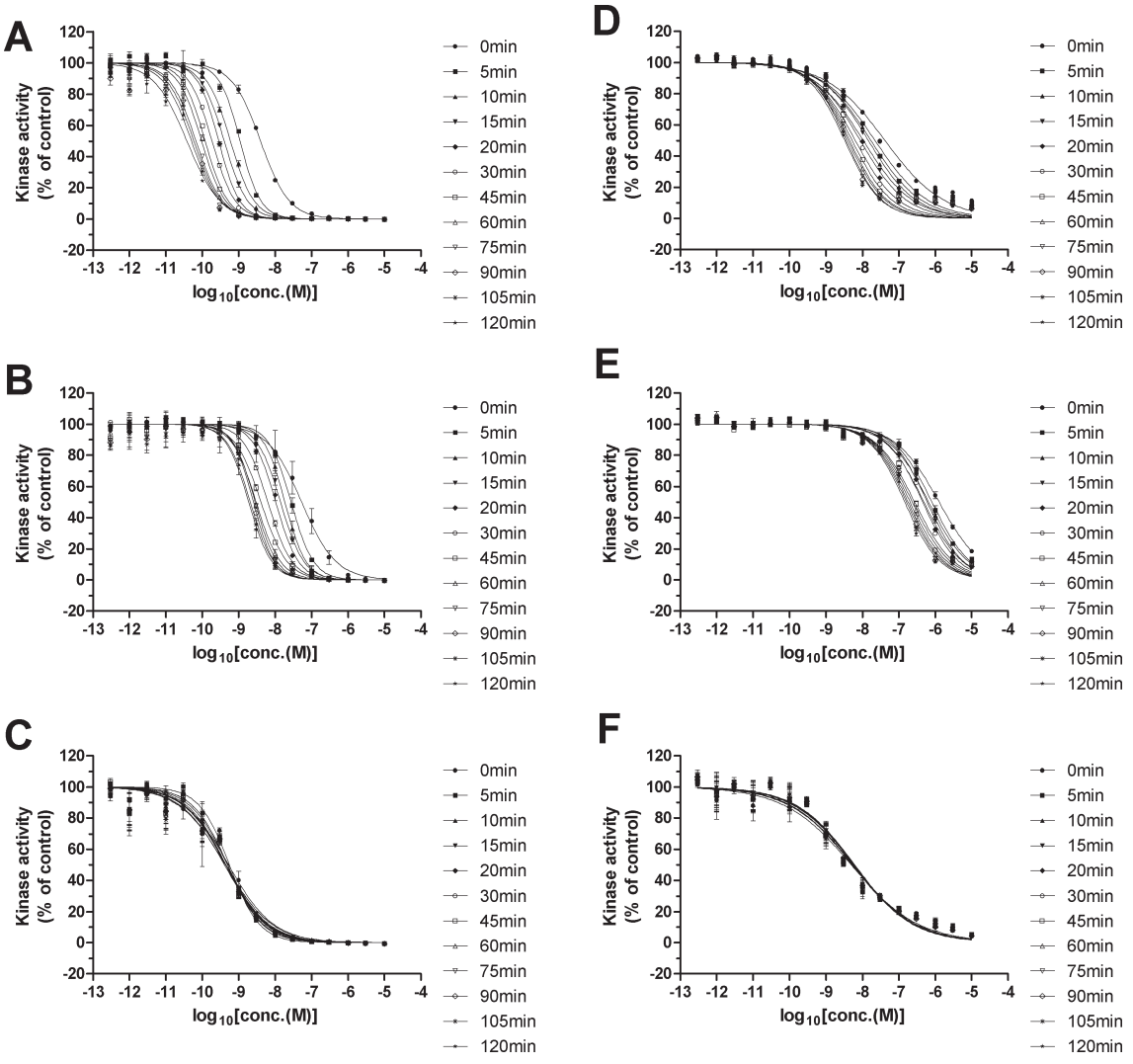

FIGURE 3: Preincubation time-dependent analysis of TAK-593 (A, D), Sorafenib (B, E), and Sunitinib (C, F). Concentration-dependent inhibitory curves at various enzyme and inhibitor preincubation times were obtained for VEGFR2 (A, B, and C) and PDGFRβ (D, E, and F). All experiments were performed by the AlphaScreen method. Data represent the mean ± SD (n = 4). Results are representative data from three independent experiments.

Table 2: Kinase Inhibition Activities with and without Preincubation

	VEGFR2 IC_{50} (nM)[a]		PDGFRβ IC_{50} (nM)[a]	
	0 min	120 min	0 min	120 min
TAK-593	4.0 (0.09)	0.036 (0.0063)	15 (2.7)	2.3 (0.36)
Sorafenib	77 (21)	1.2 (0.61)	2600 (1300)	160 (43)
Sunitinib	0.59 (0.057)	0.38 (0.063)	5.1 (3.6)	6.3 (3.9)

[a]Estimated IC_{50} values and SD in parentheses. Data are derived from three independent experiments.

same way, the hyperbolic dependency observed in Figures 4E and 6E is consistent with two-step binding of Sorafenib to VEGFR2 and PDGFRβ. The kinetic parameters for binding of Sorafenib to VEGFR2 and the kinetic parameters for binding of both inhibitors to PDGFRβ are summarized in Tables 3 and 4, respectively.

Ligand Displacement Analysis with the LanthaScreen Eu Kinase Binding Assay. In addition to the activity-based method, we performed ligand displacement analysis with a LanthaScreen Eu kinase tracer binding assay (*37*) using Alexa Fluor 647-labeled ATP-competitive type I kinase inhibitor as a tracer in order to determine the mechanism for slow binding of TAK-593 with VEGFR2 and PDGFRβ. This assay was similar to that described by Neumann et al. (*38*). A decrease of the tracer signal is caused by binding of the inhibitor. Similar to the results of activity-based preincubation experiments, TAK-593 and Sorafenib displaced the tracer in a time-dependent manner (Figure 7A,B), while Sunitinib did not (Figure 7C). Next, we performed the ligand displacement assays at inhibitor concentrations low enough to negate the contribution of probe-binding kinetics to the observed dissociation rate. When K_i is significantly higher than K_i*, eq 3 converts to linear eq 5. The kinetic constants k_4 and K_i^{*app} can be obtained by fitting of eq 5 to these data: k_4 is the y-intercept, and K_i^{*app} is calculated from the slope of the linear regression line and the k_4 value. The displacement curves (Supporting Information Figure S4A) revealed that the rate was dependent on the inhibitor concentration. Fitting of eq 7 to the displacement curves yielded k_{obs}, which was replotted versus the inhibitor concentration with fitting to eq 5 to give the upper limit of k_4 as 1.1×10^{-4} s^{-1} (Supporting Information Figure S4C). Finally, we obtained the K_i* of 570 pM for TAK-593 ligand displacement analysis. Based on the experimental design, k_4 was the rate-limiting step for dissociation of TAK-593 from the enzyme, so the apparent dissociation half-life ($t_{1/2}^{app}$) of TAK-593 and VEGFR2 was

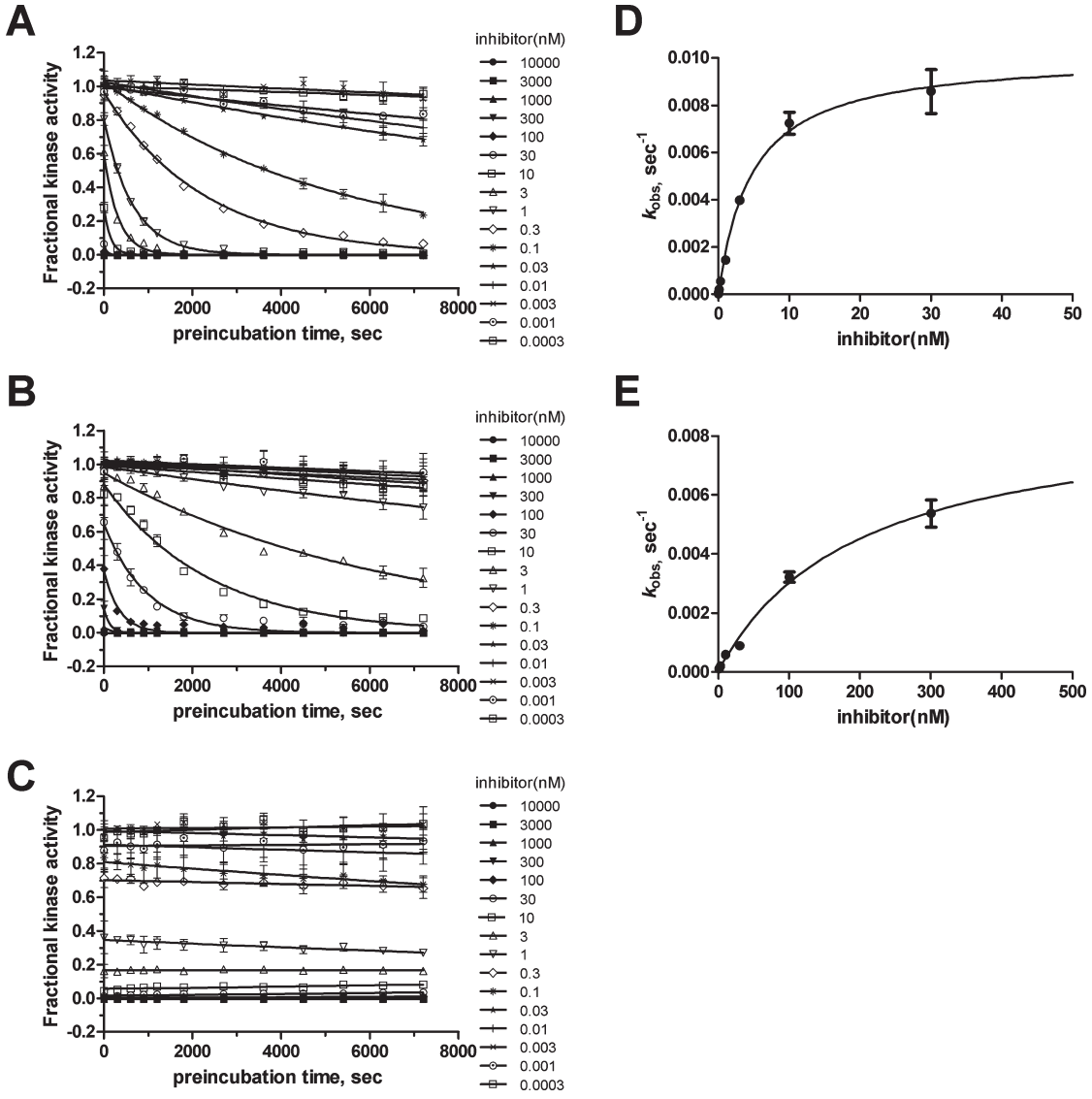

FIGURE 4: Replot of data from the activity-based preincubation analysis displayed in Figure 3 for VEGFR2 as a function of preincubation time and fitted to eq 1 to obtain k_{obs} values for TAK-593 (A), Sorafenib (B), and Sunitinib (C). Each k_{obs} value was replotted as a function of the concentration of TAK-593 (D) or Sorafenib (E) and fitted to eq 3. Because Sunitinib inhibited VEGFR2 with a different mechanism from two-step binding inhibition, the Sunitinib data were not fitted to eq 3. Data represent the mean ± SD (n = 4). These are representative plots from three independent experiments.

calculated to be approximately 130 min. Ligand displacement by Sorafenib and Sunitinib was similarly examined. As demonstrated above, Sorafenib displayed two-step binding inhibition like TAK-593 for VEGFR2 according to enzymatic activity based analysis. Accordingly, the kinetic constants for Sorafenib were obtained in the same manner as those for TAK-593 (Supporting Information Figure S4B,D). In contrast, inhibition of VEGFR2 by Sunitinib did not show time dependence (Figure 7C), so this two-step binding analysis was not suitable for Sunitinib. As well, ligand displacement analysis against PDGFRβ was performed in the same manner as for VEGFR2 (Figure 7D−F and Supporting Information Figure S5). The kinetic constants obtained from these analyses are summarized in Tables 3 and 4.

100-Fold Dilution Assay for Determining Dissociation Rate Constants for VEGFR2 and PDGFRβ by the Activity-Based Method. The dissociation rate constants (k_{off}) of the inhibitors were examined by a rapid large dilution method (*39*). Dilution was of sufficient magnitude to reduce the inhibitor concentration to well below apparent K_i at a saturating ATP concentration. Under such conditions, inhibitor dissociation is an irreversible event. As shown in Figure 8A, within the time limit of the assay, the product formation rate of the VEGFR2 enzyme reaction in the presence of Sunitinib was the same as that of the control reaction and consistent with a rapid binding mechanism. Accordingly, the recovery of enzymatic activity was too rapid to determine the dissociation rate constant of Sunitinib accurately ($k_{off} > 0.693/5$ min $= 2.3 \times 10^{-3}$ s^{-1}) (Table 5). In contrast, preincubation of VEGFR2 with TAK-593 or Sorafenib resulted in undetectable catalytic activity for 90 min after dilution. The dissociation rate constant of Sorafenib from VEGFR2 and its $t_{1/2}$ value were 3.3×10^{-5} s^{-1} and 370 min, respectively (Table 5), while the dissociation rate constant of TAK-593 from VEGFR2 and its $t_{1/2}$ value were 2.5×10^{-6} s^{-1} and 5100 min, respectively (Table 5). Dissociation of TAK-593 from VEGFR2 was so slow that our determination of k_{off} reflected the upper limit of its rate. Clearly, the dissociation of TAK-593 was much slower than that of either Sunitinib or Sorafenib. For TAK-593, the $t_{1/2}$ value obtained by this dilution method was much longer

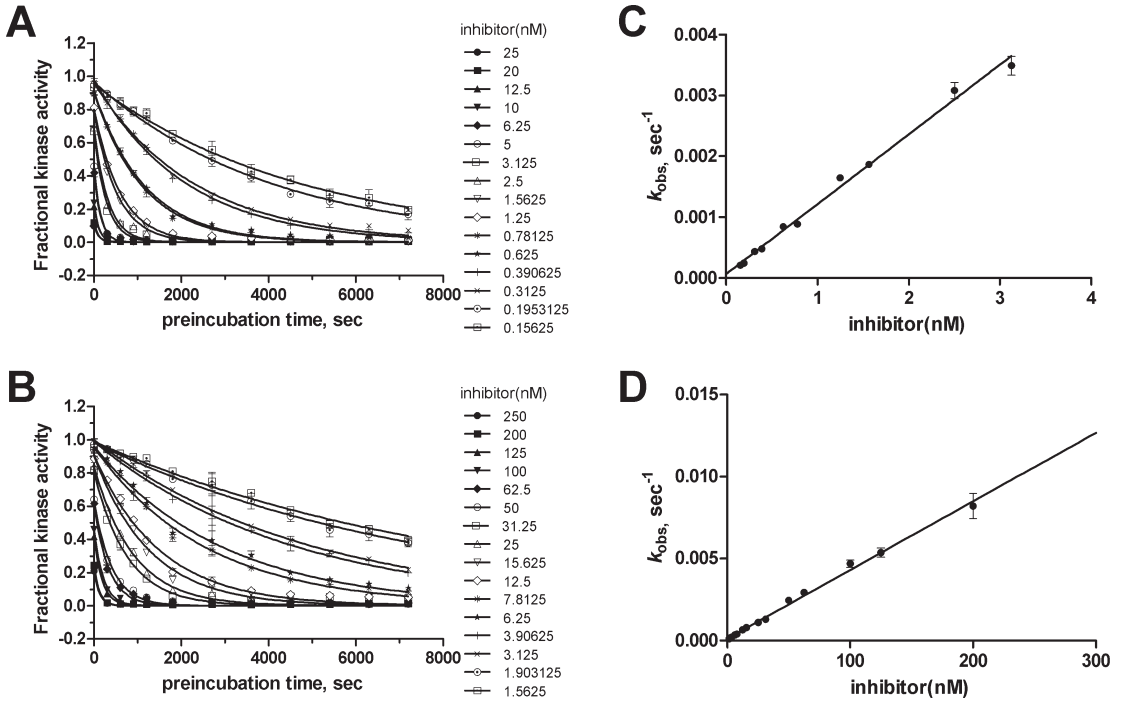

FIGURE 5: Replot of data from the activity-based preincubation analysis for inhibition of VEGFR2 by TAK-593 (A) and Sorafenib (B) at low concentrations. The k_{obs} values were replotted as a function of the concentration of TAK-593 (C) or Sorafenib (D) and fitted to eq 5. Data represent the mean ± SD (n = 4). These are representative plots from three independent experiments.

Table 3: Kinetic Constants for VEGFR2 from Activity-Based Preincubation Assays and Fluorescent Ligand Displacement Assays

	method	K_i (nM)[a]	K_i* (nM)	slope (M^{-1} s^{-1})[a]	k_3 (s^{-1})[a]	k_4 (s^{-1})[a]	$t_{1/2}^{app}$ (min)[d]
TAK-593	activity based	3.2 (0.98)	0.025[b]	1.0×10^6 (8.7×10^4)	1.0×10^{-2} (1.8×10^{-3})	7.8×10^{-5} (1.3×10^{-5})	150 (23)
	ligand displacement	ND	0.57[c]	9.9×10^4 (3.0×10^3)	ND	1.1×10^{-4} (6.9×10^{-5})	130 (65)
Sorafenib	activity based	69 (26)	0.97[b]	3.5×10^4 (6.2×10^3)	8.5×10^{-3} (9.8×10^{-4})	1.2×10^{-4} (2.1×10^{-5})	96 (17)
	ligand displacement	ND	5.0[c]	4.6×10^3 (1.1×10^2)	ND	4.6×10^{-5} (3.7×10^{-5})	350 (90)
Sunitinib[e]	activity based	ND	ND	ND	ND	ND	ND
	ligand displacement	ND	ND	ND	ND	ND	ND

[a]Estimated values and SD in parentheses. [b]Values calculated with eq 4 using K_I, k_3, and k_4 values. [c]Values calculated with eq 5 using k_4 values. [d]Estimated values and SD in parentheses calculated with eq 7 using k_4. [e]Since Sunitinib did not show slow binding inhibition, these analyses were not applicable. These results are derived from three independent experiments.

than the value obtained by the preincubation time-dependent assay (Tables 3 and 5). There could be at least two reasons for the discrepancy between the observed dissociation rate constants. First, this type of dilution assay only monitors the dissociation step, as described above, while the preincubation time-dependent assay monitors both association and dissociation, with the association rate placing a lower limit on the magnitude of k_{obs}. Second, it is difficult to determine the difference between zero and a value close to zero by replot analysis of preincubation time-dependent assay data when the dissociation rate constant is extremely small. Finally, using $k_3 = 1.0 \times 10^{-2}$ s^{-1} and $K_i = 3.2$ nM from our preincubation analysis (Table 3), as well as k_4 (k_{off}) = 2.5×10^{-6} s^{-1} from the activity-based enzyme−inhibitor complex rapid large dilution assay, K_i * of TAK-593 for VEGFR2 was calculated to be 0.8 pM by using eq 5. Sunitinib dissociated very quickly from PDGFRβ after rapid dilution in the same manner as from VEGFR2 (Figure 8B). In this experiment, the dissociation rate of TAK-593 from PDGFRβ was revealed to be slightly faster than that of Sorafenib, with the dissociation rate constants of TAK-593 and Sorafenib being 4.5×10^{-5} and 1.3×10^{-5} s^{-1}, respectively (Table 5). Using eq 7, the $t_{1/2}$ values of TAK-593 and Sorafenib were calculated to be 260 and 870 min, respectively (Table 5).

100-Fold Dilution Assay for Determining Dissociation Rate Constants for VEGFR2 and PDGFRβ by the Kinase Tracer Binding-Based Method. We also determined the dissociation rate constants by a ligand displacement method to confirm the dissociation kinetics of TAK-593, Sunitinib, and Sorafenib (Figure 8C,D). Once again, dissocation of Sunitinib from VEGFR2 displayed rapid equilibrium, with the probe kinetics determining the rate. In contrast, TAK-593 and Sorafenib dissociated slowly from VEGFR2 (Figure 8C). By fitting eq 9 to the displacement curves, we obtained the dissociation rate constants. As observed with the activity-based dilution method, the $t_{1/2}$ of TAK-593 and Sorafenib was determined to be 65 h and 280 min, respectively (Table 5). These results confirmed that TAK-593 dissociates from VEGFR2 very slowly. Sunitinib dissociated rapidly from PDGFRβ in the same manner as from VEGFR2 (Figure 8D). Similar to the results of the activity-based dilution assay, dissociation of TAK-593 was revealed to be faster than that of Sorafenib, with the k_{off} value and $t_{1/2}$ of TAK-593 for PDGFRβ being 2.4×10^{-5} s^{-1} and 500 min, respectively (Table 5). Dissociation of Sorafenib from PDGFRβ was too slow for us to determine the dissociation rate constant (calculated as the upper limit).

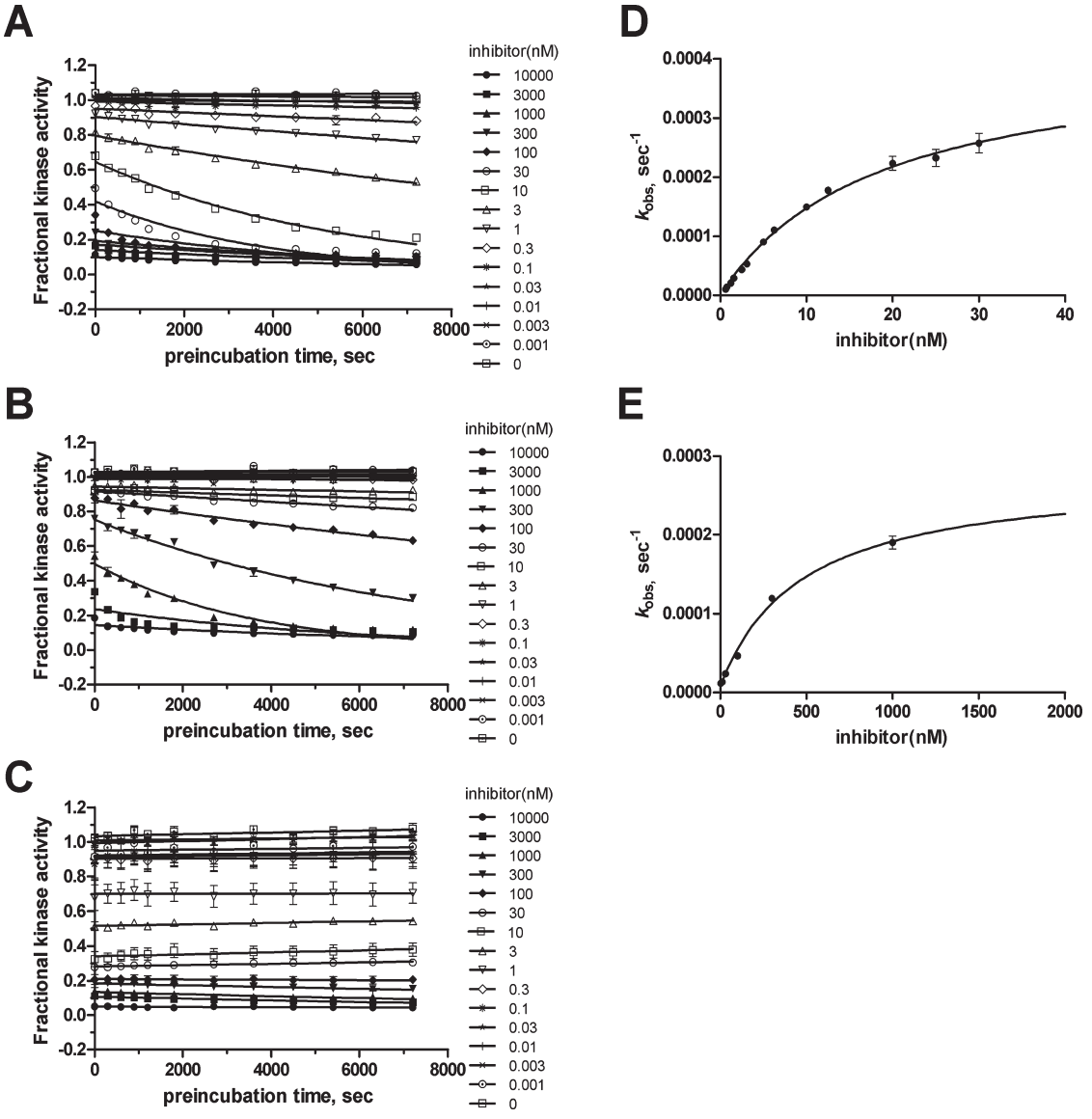

FIGURE 6: Replot of data from the activity-based preincubation analysis displayed in Figure 3, showing inhibition of PDGFRβ as a function of preincubation time and fitted to eq 1 to obtain k_{obs} values for TAK-593 (A), Sorafenib (B), and Sunitinib (C). Each k_{obs} value was replotted as a function of the concentration of TAK-593 (D) or Sorafenib (E) and fitted to eq 5. Because Sunitinib inhibited PDGFRβ with a different mechanism from two-step binding inhibition, the Sunitinib data were not fitted to eq 3. Data represent the mean ± SD (n = 4). These are representative plots from three independent experiments.

Table 4: Kinetic Constants for PDGFRβ from Activity-Based Preincubation Assays and Fluorescent Ligand Displacement Assays

	method	K_i (nM)[a]	K_i* (nM)	slope (M^{-1} s^{-1})[a]	k_3 (s^{-1})[a]	k_4 (s^{-1})[a]	$t_{1/2}^{app}$ (min)[d]
TAK-593	activity based	4.5 (1.6)	0.39[b]	1.6×10^4 (3.3×10^3)	3.0×10^{-4} (6.9×10^{-5})	2.6×10^{-5} (1.3×10^{-5})	510 (220)
	ligand displacement	ND	3.5[c]	5.5×10^3 (1.1×10^3)	ND	3.9×10^{-5} (3.1×10^{-5})	430 (250)
Sorafenib	activity based	270 (60)	7.1[b]	320 (50)	3.9×10^{-4} (1.6×10^{-4})	1.0×10^{-5} (6.2×10^{-6})	1300 (580)
	ligand displacement	ND	$\ll$52[e]	190 (15)	ND	$\ll 1.0 \times 10^{-5}$ [e]	$\gg$1200[e]
Sunitinib[f]	activity based	ND	ND	ND	ND	ND	ND
	ligand displacement	ND	ND	ND	ND	ND	ND

[a]Estimated values and SD in parentheses. [b]Values calculated with eq 4 using K_i, k_3, and k_4 values. [c]Values calculated with eq 5 using k_4 values. [d]Estimated values and SD in parentheses calculated with eq 7 using k_4. [e]Due to limitations of the assay system, K_i* and $t_{1/2}^{app}$ were calculated using k_4 as 1.0×10^{-5}. [f]Since Sunitinib did not show slow binding inhibition, these analyses were not applicable. These results are derived from three independent experiments.

DISCUSSION

TAK-593 is a novel VEGFR/PDGFR inhibitor with high potency and high selectivity. TAK-593 only inhibited B-Raf modestly with an IC_{50} value of 8400 nM, so its inhibitory spectrum against protein kinases or cancer cells was predicted to differ from that of Sorafenib since Sorafenib reportedly inhibits B-Raf and VEGFR2 almost equally (*40*). With respect to other kinases outside the PDGFR and FGFR superfamily, TAK-593 potently inhibited Abl among wild-type kinases and mutant tyrosine

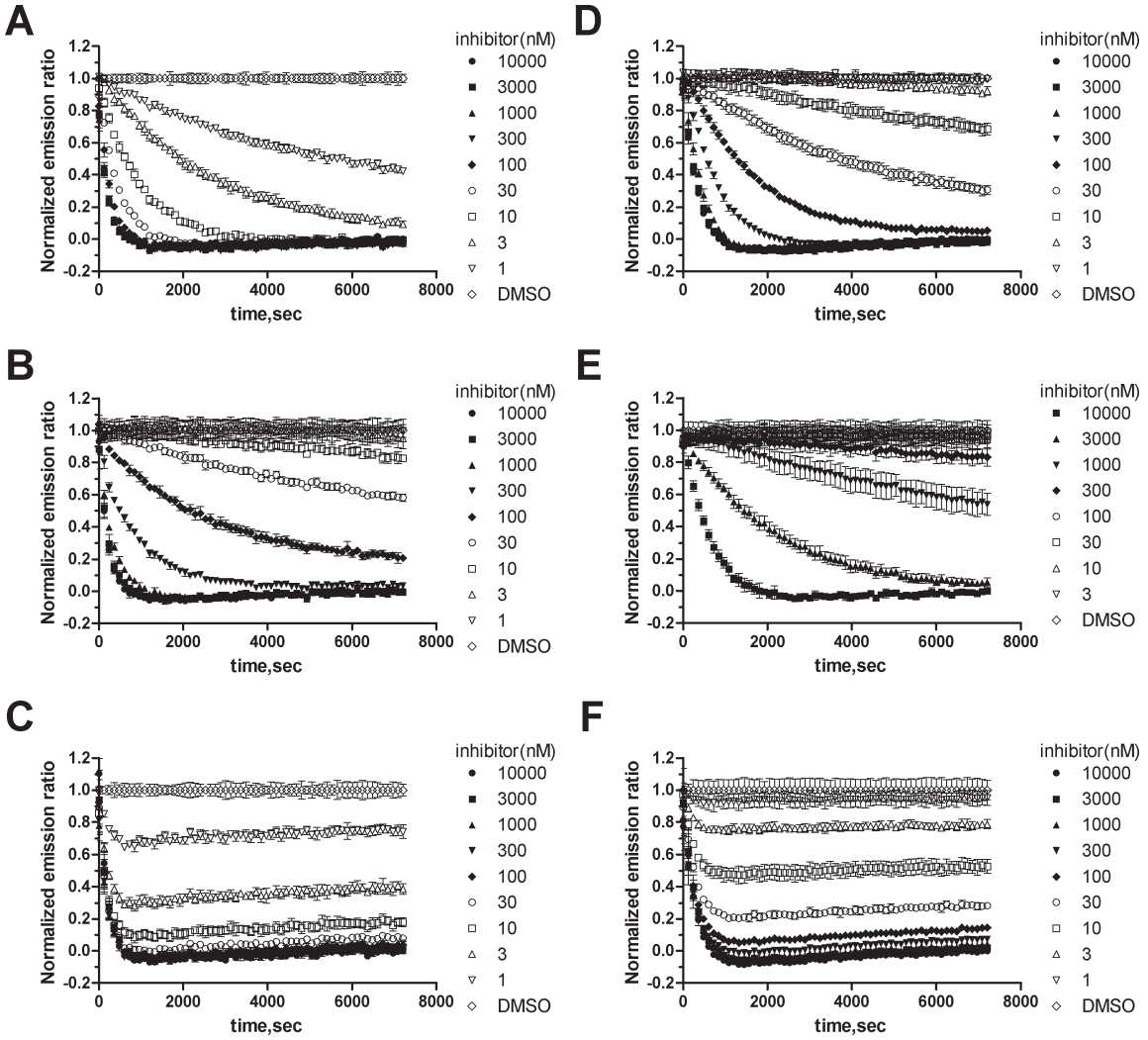

FIGURE 7: Displacement of the fluorescent tracer from VEGFR2 (A, B, and C) and PDGFRβ (D, E, and F) monitored in real time at various concentrations of TAK-593 (A, D), Sorafenib (B, E), and Sunitinib (C, F) for determination of k_{obs} (the rate constant for the onset of inhibition). Data represent the mean ± SD (n = 4). These are representative plots from three independent experiments.

kinases such as c-Kit (V560G), PDGFRα (V561D), and Abl (M351T). Some kinase mutations observed in cancer cells result in gain of function that drives tumor proliferation or leads to resistance against the clinically available kinase inhibitors. For example, c-Kit and PDGFRα mutations are common in most GIST patients (*41*), and c-Kit (V560G) is reported to increase sensitivity to imatinib (*42*). Therefore, TAK-593 may inhibit the proliferation of GIST in the same manner as imatinib. On the other hand, Abl (M351T) was discovered in chronic myelogenous leukemia (CML) and was reported to increase imatinib resistance (*43*). Treatment with TAK-593 may be particularly efficacious for CML, especially in patients with imatinib-resistant disease, because TAK-593 inhibits both wild-type Abl and the imatinib-resistant mutant of Abl.

Many protein kinases are regulated through phosphorylation at specific sites (such as an activation loop), leading to changes of their conformation and enzymatic activation (*15*). In general, phosphorylated kinases adopt an active conformation, and unphosphorylated kinases adopt an inactive conformation. Type II kinase inhibitors preferentially bind with the inactive form of the enzyme, possibly trapping the enzyme in the inactive state, which may contribute to a higher potency in cellular assays or in vivo. Keeping this in mind, during the course of compound optimization, we often performed assays with the unphosphorylated/inactive enzyme and assessed its basal catalytic activity. Furthermore, we are required to evaluate inhibitory activity of type II inhibitors within a short reaction time since most of type II kinase inhibitors display time dependency with their inhibition and preferably inhibit nonphosphorylated enzyme. Therefore, if we choose an assay method with long reaction time, as nonphosphorylated enzyme decreases and phosphorylated enzyme increases, we may underestimate the inhibitory effects or misunderstand the slow binding mechanism of type II kinase inhibitors. To address these necessities, we performed enzyme assays in AlphaScreen platform that may be desired high sensitivity and performed with $MnCl_2$ containing buffer in addition to $MgCl_2$ since autophosphorylation activity of VEGFR2 increased (*44*). Promising compounds were then examined for time-dependent binding in addition to overall affinity. In the present study, TAK-593 and Sorafenib inhibited VEGFR2 and PDGFRβ in a time-dependent manner, while Sunitinib did not. After 120 min of preincubation, TAK-593 inhibited VEGFR2 and PDGFRβ more potently than the other two inhibitors examined. TAK-593 and Sorafenib interacted with VEGFR2 in a similar manner, accessing the deeper region of the ATP-binding pocket of the enzyme, which is often called the back pocket or the DFG-out site. Such binding might be necessary for time-dependent inhibition but may not be sufficient since we have observed some inhibitors that interact

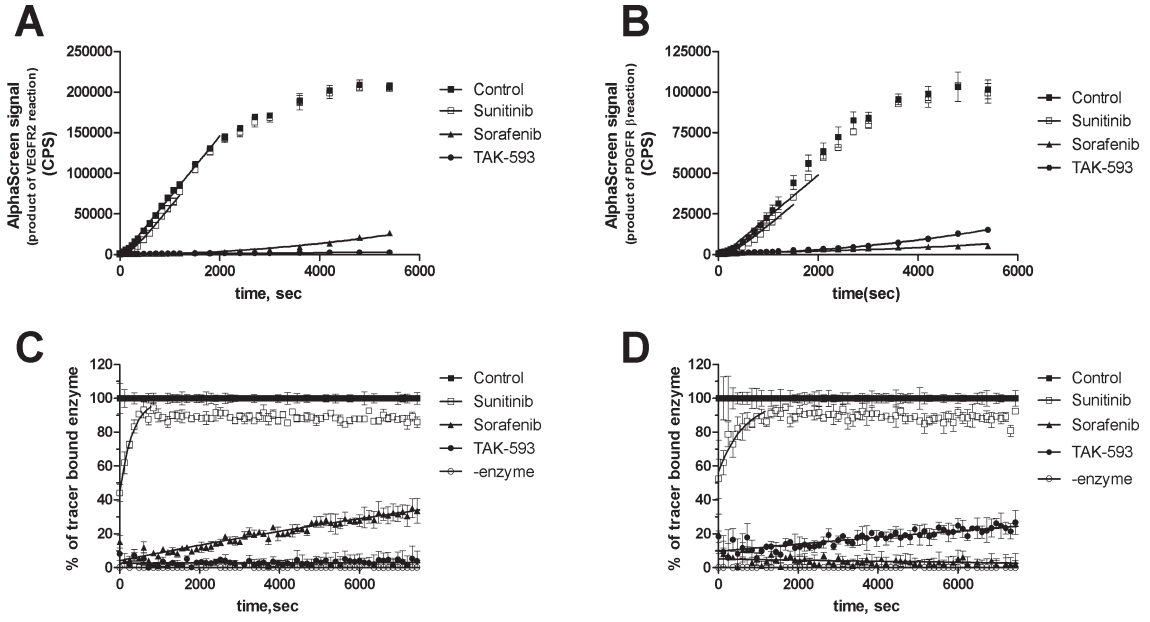

FIGURE 8: Recovery of enzyme activity (A and B) and tracer binding activity (C and D) after 100-fold dilution for estimation of dissociation rate constants. (A) The 100-fold dilution assay for VEGFR2 with TAK-593 (●), Sorafenib (▲), or Sunitinib (□) and without any inhibitor as a control (■). (B) The 100-fold dilution assay for PDGFRβ with TAK-593 (●), Sorafenib (▲), or Sunitinib (□) and without any inhibitor as a control (■). All experiments were performed by the AlphaScreen method. These are representative plots from three independent experiments. Data represent the mean ± SD ($n = 3$). (C) The 100-fold dilution assay for VEGFR2 with TAK-593 (●), Sorafenib (▲), or Sunitinib (□), without any inhibitor as a control (■), and without inhibitor or enzyme (○). (D) The 100-fold dilution assay for PDGFRβ with TAK-593 (●), Sorafenib (▲), or Sunitinib (□), without any inhibitor as a control (■), and without inhibitor or enzyme (○). These are representative plots from three independent experiments. Data represent the mean ± SD ($n = 4$).

Table 5: Kinetic Constants for VEGFR2 and PDGFRβ from Enzyme−Inhibitor Complex Dilution Assays

		VEGFR2		PDGFRβ	
	method	k_{off} (s^{-1})[a]	$t_{1/2}$ (min)[b]	k_{off} (s^{-1})[a]	$t_{1/2}$ (min)[b]
TAK-593	activity based	2.5×10^{-6} (1.2×10^{-6})	5100 (1900)	4.5×10^{-5} (7.3×10^{-6})	260 (40)
	ligand displacement	2.9×10^{-6} (3.3×10^{-8})	3900 (44)	2.4×10^{-5} (6.3×10^{-6})	500 (130)
Sorafenib	activity based	3.3×10^{-5} (8.8×10^{-6})	370 (120)	1.3×10^{-5} (2.0×10^{-6})	870 (140)
	ligand displacement	4.1×10^{-5} (3.4×10^{-6})	280 (24)	ND[c]	ND[c]
Sunitinib	activity based	$> 2.3 \times 10^{-3}$ [d]	< 5	$> 2.3 \times 10^{-3}$ [d]	< 5
	ligand displacement	3.9×10^{-3} (1.6×10^{-3})	3 (1)	1.4×10^{-3} (1.2×10^{-4})	8 (1)

[a]Estimated k_{off} values and SD in parentheses. [b]Values calculated with eq 7 using k_{off} and SD in parentheses. [c]Because Sorafenib dissociated from PDGFRβ very slowly, we were not able to obtain k_{off} or $t_{1/2}$. [d]Values calculated with eq 7 using $t_{1/2}$ of less than 5 min. These results are derived from three independent experiments.

with the back pocket site but do not display slow binding. As shown in Table 1, TAK-593 inhibits other kinases less potently than those of the VEGFR and PDGFR family. We cannot predict that TAK-593 will inhibit all of these kinases in the same manner as VEGFR2 and PDGFRβ, since very few kinases are known to adopt the DFG-out conformation of their activation loop with or without an inhibitor (*18*). STI-571, an Abl inhibitor reported as the first type II kinase inhibitor, binds to c-Kit and Abl in the same manner (DFG-out conformation) but binds to SYK differently (DFG-in conformation) (*45*).

Like other type II inhibitors, TAK-593 displayed slow binding to VEGFR2 and PDGFRβ. We determined that TAK-593 rapidly formed an initial complex with VEGFR2, with a K_i of 3.2 nM, and then slowly proceeded to a tight complex with a K_i* of 0.025 nM at equilibrium. From these values, and the Gibbs free energy equation ($\Delta G = -RT \ln(K_i^*/K_i)$), the free energy of transition from the initial complex EI to the more stable complex EI* was calculated to be 2.86 kcal/mol at 25 °C. Analysis of the crystal structure of the VEGFR2 complex with TAK-593 revealed that VEGFR2 existed in the inactive DFG-out conformation (data not shown). From our results, the DFG-out conformation of the TAK-593 and VEGFR2 complex may be more stable than the active DFG-in conformation, contributing to slow dissociation of TAK-593 with VEGFR2 protein isomerization. However, further studies will be needed to clarify the relationship between biochemical parameters and protein conformational changes.

In this study, we determined the kinetic constants of Sorafenib and Sunitinib as well as TAK-593 through a binding assay based on fluorescent-labeled tracer displacement, in addition to using the conventional method based on enzymatic activity. The chief advantage of the displacement binding assay over an activity-based assay is that there is no change from unphosphorylated to phosphorylated kinase throughout the assay period. Thus, we could obtain kinetic constants for a single state of the enzyme, i.e., the unphosphorylated state. Enzymatic activity introduces the possibility of autophosphorylation during analysis. Therefore, there might be some uncertainty in the results of activity-based assays because we cannot control autophosphorylation.

With respect to VEGFR2, comparing the kinetic constants calculated from activity-based preincubation assays and the constants obtained from ligand displacement-based assays, the K_i* values (the true affinity of the inhibitor) were not in good agreement. In fact, there was about a 23-fold difference between the activity-based and ligand displacement-based K_i* values in the case of TAK-593 and about a 5-fold difference in the case of Sorafenib. This discrepancy may be mainly related to the difference of the on-rate (the slope obtained by linear regression analysis of k_{obs} at the low concentration of inhibitor) in each method. According to activity-based analysis, the on-rate of TAK-593 was determined to be about 1.0×10^6 M^{-1} s^{-1}, as the slope obtained with eq 5 (Table 3). On the other hand, the on-rate was determined to be 9.9×10^4 M^{-1} s^{-1} by binding-based analysis (Table 3) and was about a 10-fold difference of these on-rates for TAK-593. Similarly, the on-rate of Sorafenib was determined to be about 3.5×10^4 M^{-1} s^{-1} by activity-based analysis, and the on-rate obtained with ligand displacement-based analysis was about 4.6×10^3 M^{-1} s^{-1}. There was about a 7.5-fold difference of the on-rates for Sorafenib.

In the case of PDGFRβ, there was about a 9-fold difference between the activity-based and ligand displacement-based K_i* values for TAK-593. The on-rate of TAK-593 was determined to be about 1.6×10^4 M^{-1} s^{-1} by activity-based analysis and was about 5.5×10^3 M^{-1} s^{-1} by ligand displacement-based analysis (Table 4), so there was about a 2.9-fold difference of these on-rates for TAK-593. As the discrepancy of the on-rates for the inhibitor was smaller, each K_i* value seemed to be in better agreement.

Several reasons can be considered for the discrepancy of the on-rates obtained by each analysis. First, we did not consider the kinetic constant of the fluorescent tracer, so we could not determine all of the kinetic constants of the inhibitors in the ligand displacement assay. Second, the ligand displacement assay used an Eu-labeled anti-His-tag antibody against the His tag on the kinase protein. Interaction of the antibody with the kinase might have altered the conformation of the enzyme, so that the on-rate of the inhibitor was slower than the on-rate for the free kinase enzyme. At present, we cannot define the reasons for the discrepancy of the K_i* values and on-rates.

TAK-593 dissociated very slowly from VEGFR2 and PDGFRβ. For VEGFR2, the dissociation half-life of TAK-593 was calculated to be 85 h in the activity-based dilution assay and 65 h in the ligand displacement-based dilution assay. These half-life data of both assays were in good agreement. When dissociation from PDGFRβ was assessed by the ligand displacement-based dilution assay, the dissociation rate constant of each inhibitor was a little smaller than the rate constants obtained by the activity-based dilution method, especially for Sorafenib. These discrepancies may have been due to differences of the phosphorylation of PDGFRβ in each reaction. As described above, some receptor tyrosine kinases (including VEGFR2 and PDGFRβ) show autophosphorylation when stimulated by ligands in intact cells or during a recombinant enzyme reaction. Thus, both unphosphorylated and phosphorylated kinase are assessed by the activity-based assay, and the ratio of each enzyme is constantly shifting through the assay period. On the other hand, there is no change in the phosphorylation state of kinases assayed by the ligand displacement method, so if the affinity for the unphosphorylated kinase is lower than that for the phosphorylated kinase, discrepancies may appear. However, there is good overall agreement between the dissociation rate constants from activity-based dilution assays and those from ligand displacement-based dilution assays. There are also limitations of each method, such as minimal dissociation or reactivation of the enzyme. In addition to evaluating the slow onset to full inhibition by TAK-593 we must be mindful to examine if the binding system strays into tight binding conditions defined as invalidating the approximation that free inhibitor concentration = total inhibitor concentration. A hallmark of straying into inhibitor tight binding conditions is the observation in an inhibitor dose−response curve of a greater than unity Hill slope that increases in value as the concentration of competitive substrate decreases. We did not observe such a phenomenon, but to confirm our experiments remained under relaxed binding, we conducted a numerical simulation of TAK-593 binding to VEGFR2 using the parameters obtained from our progress curve analysis described above. The numerical simulation explicitly solves for free inhibitor concentration and is valid under any arbitrary ratio of inhibitor to enzyme concentrations as well as any ratio of enzyme concentration to K_I. The simulated outcome fit well to our experimental observations (Supporting Information), further confirming that our analysis produced reliable values.

Finally, to confirm reversible inhibition VEGFR2 by TAK-593, LC/MS analysis was done. There was no evidence of chemical binding-based irreversibility (data not shown), consistent with the lack of a chemically reactive moiety in the structure of TAK-593. Thus, we concluded that TAK-593 has a unique binding and dissociation profile, with slow two-step binding inhibition of VEGFR2 and PDGFRβ. In the case of VEGFR2, TAK-593 has a much longer residence time than Sunitinib and Sorefenib. From the results of enzymatic activity-based and fluorescent-labeled tracer displacement-based dilution assays, TAK-593 has a longer residence time on PDGFRβ than Sunitinib, but the residence time of TAK-593 is shorter than that of Sorafenib. Accordingly, TAK-593 may have different kinase inhibitory properties from Sorafenib in addition to a different kinase selectivity profiles.

As described above, slow dissociation may contribute to higher in vitro cellular activity, since a small dissociation rate constant contributes to the affinity of the inhibitor at equilibrium and the duration of inhibition once the inhibitor has bound to the targeted protein. Thus, TAK-593 may inhibit the VEGFR and PDGFR signaling pathways for longer than rapidly dissociating inhibitors in cellular assays. Slow reversible inhibition may also contribute to efficacy in vivo (*24*, *46*), especially since a slow off-rate is independent of the concentrations of inhibitor and the target protein as well as other factors such as absorption, distribution, and clearance. A long dissociation half-life may also contribute to an enhanced duration of action on the target enzyme, requiring lower doses of the drug in vivo. Lower doses will reduce inhibition of off-target enzymes and unexpected side effects. This may be an added advantage of TAK-593, in addition to its high potency against target kinases and its high selectivity.

From our results, TAK-593 may be the ultimate physiological inhibitor (*47*) for VEGFR2, and it is similar to the recent report of Axitinib toward VEGFR2 catalytic domain with juxtamembrane region (*22*). TAK-593 may well persistently inhibit VEGFR2 until turnover of the enzyme occurs in target cells. In conclusion, TAK-593 is a highly selective, potent, and ATP-competitive VEGFR/PDGFR inhibitor with a two-step slow binding mechanism. Moreover, TAK-593 has one of the longest residence times of any VEGFR inhibitor yet reported. Based on these findings, TAK-593 is a promising inhibitor for VEGFRs and PDGFRs that might have a prominent and durable effect at very low doses in vivo.

ACKNOWLEDGMENT

We thank Taeko Yoshida for kind assistance with the enzymatic assays and Ikuo Miyahisa for helpful discussion about data analysis for the kinetic assays. We thank Naoki Miyamoto and Takaharu Hirayama for preparing the compounds tested. We also thank Junji Matsui and Naoki Tarui for encouragement to undertake this study.

SUPPORTING INFORMATION AVAILABLE

Amino acid sequences of VEGFR2 and PDGFRβ (Figure S1), concentration-dependent inhibitory curves of TAK-593 for VEGFR1, VEGFR2, VEGFR3, PDGFRα, PDGFRβ, and c-kit (Figure S2), replot data from the activity-based preincubation analysis of PDGFRβ at low inhibitor concentrations (Figure S3), displacement of fluorescent tracer at low inhibitor concentrations for VEGFR2 and PDGFRβ (Figures S4 and S5, respectively), simulations of TAK-593-VEGFR2 association progress curves by use of differential equations (Figures S6−S9), details of the reaction conditions for each kinase (Table S1), and the results obtained with KinaseProfiler (Millipore), a large kinase panel, and 1 μM of TAK-593 (Table S2). This material is available free of charge via the Internet at http://pubs.acs.org.

REFERENCES

1. Folkman, J. (1990) What is the evidence that tumors are angiogenesis dependent? *J. Natl. Cancer Inst. 82*, 4–6.
2. Thomas, K. A. (1996) Vascular endothelial growth factor, a potent and selective angiogenic agent. *J. Biol. Chem. 271*, 603–606.
3. Olsson, A. K., Dimberg, A., Kreuger, J., and Claesson-Welsh, L. (2006) VEGF receptor signalling—in control of vascular function. *Nat. Rev. Mol. Cell Biol. 7*, 359–371.
4. Chung, A. S., Lee, J., and Ferrara, N. (2010) Targeting the tumour vasculature: insights from physiological angiogenesis. *Nat. Rev. Cancer 10*, 505–514.
5. Underiner, T. L., Ruggeri, B., and Gingrich, D. E. (2004) Development of vascular endothelial growth factor receptor (VEGFR) kinase inhibitors as anti-angiogenic agents in cancer therapy. *Curr. Med. Chem. 11*, 731–745.
6. Sloan, B., and Scheinfeld, N. S. (2008) Pazopanib, a VEGF receptor tyrosine kinase inhibitor for cancer therapy. *Curr. Opin. Invest. Drugs 9*, 1324–1335.
7. Cai, Z. W., Zhang, Y., Borzilleri, R. M., Qian, L., Barbosa, S., Wei, D., Zheng, X., Wu, L., Fan, J., Shi, Z., Wautlet, B. S., Mortillo, S., Jeyaseelan, R., Sr., Kukral, D. W., Kamath, A., Marathe, P., D'Arienzo, C., Derbin, G., Barrish, J. C., Robl, J. A., Hunt, J. T., Lombardo, L. J., Fargnoli, J., and Bhide, R. S. (2008) Discovery of brivanib alaninate ((*S*)-((*R*)-1-(4-(4-fluoro-2-methyl-1*H*-indol-5-yloxy)-5-methylpyrrolo[2,1-*f*][1,2,4]triazin-6-yloxy)propan-2-yl)2-aminopropanoate), a novel prodrug of dual vascular endothelial growth factor receptor-2 and fibroblast growth factor receptor-1 kinase inhibitor (BMS-540215). *J. Med. Chem. 51*, 1976–1980.
8. Yu, J., Ustach, C., and Kim, H. R. (2003) Platelet-derived growth factor signaling and human cancer. *J. Biochem. Mol. Biol. 36*, 49–59.
9. Heinrich, M. C., Blanke, C. D., Druker, B. J., and Corless, C. L. (2002) Inhibition of KIT tyrosine kinase activity: a novel molecular approach to the treatment of KIT-positive malignancies. *J. Clin. Oncol. 20*, 1692–1703.
10. Chow, L. Q., and Eckhardt, S. G. (2007) Sunitinib: from rational design to clinical efficacy. *J. Clin. Oncol. 25*, 884–896.
11. Chang, Y. S., Adnane, J., Trail, P. A., Levy, J., Henderson, A., Xue, D., Bortolon, E., Ichetovkin, M., Chen, C., McNabola, A., Wilkie, D., Carter, C. A., Taylor, I. C., Lynch, M., and Wilhelm, S. (2007) Sorafenib (BAY 43-9006) inhibits tumor growth and vascularization and induces tumor apoptosis and hypoxia in RCC xenograft models. *Cancer Chemother. Pharmacol. 59*, 561–574.
12. Hubbard, S. R., and Till, J. H. (2000) Protein tyrosine kinase structure and function. *Annu. Rev. Biochem. 69*, 373–398.
13. Blume-Jensen, P., and Hunter, T. (2001) Oncogenic kinase signalling. *Nature 411*, 355–365.
14. Hubbard, S. R., Mohammadi, M., and Schlessinger, J. (1998) Autoregulatory mechanisms in protein-tyrosine kinases. *J. Biol. Chem. 273*, 11987–11990.
15. Liu, Y., and Gray, N. S. (2006) Rational design of inhibitors that bind to inactive kinase conformations. *Nat. Chem. Biol. 2*, 358–364.
16. Schindler, T., Bornmann, W., Pellicena, P., Miller, W. T., Clarkson, B., and Kuriyan, J. (2000) Structural mechanism for STI-571 inhibition of abelson tyrosine kinase. *Science 289*, 1938–1942.
17. Nagar, B., Bornmann, W. G., Pellicena, P., Schindler, T., Veach, D. R., Miller, W. T., Clarkson, B., and Kuriyan, J. (2002) Crystal structures of the kinase domain of c-Abl in complex with the small molecule inhibitors PD173955 and imatinib (STI-571). *Cancer Res. 62*, 4236–4243.
18. Kufareva, I., and Abagyan, R. (2008) Type-II kinase inhibitor docking, screening, and profiling using modified structures of active kinase states. *J. Med. Chem. 51*, 7921–7932.
19. Pargellis, C., Tong, L., Churchill, L., Cirillo, P. F., Gilmore, T., Graham, A. G., Grob, P. M., Hickey, E. R., Moss, N., Pav, S., and Regan, J. (2002) Inhibition of p38 MAP kinase by utilizing a novel allosteric binding site. *Nat. Struct. Biol. 9*, 268–272.
20. Wood, E. R., Truesdale, A. T., McDonald, O. B., Yuan, D., Hassell, A., Dickerson, S. H., Ellis, B., Pennisi, C., Horne, E., Lackey, K., Alligood, K. J., Rusnak, D. W., Gilmer, T. M., and Shewchuk, L. (2004) A unique structure for epidermal growth factor receptor bound to GW572016 (Lapatinib): relationships among protein conformation, inhibitor off-rate, and receptor activity in tumor cells. *Cancer Res. 64*, 6652–6659.
21. Petrov, K. G., Zhang, Y. M., Carter, M., Cockerill, G. S., Dickerson, S., Gauthier, C. A., Guo, Y., Mook, R. A., Jr., Rusnak, D. W., Walker, A. L., Wood, E. R., and Lackey, K. E. (2006) Optimization and SAR for dual ErbB-1/ErbB-2 tyrosine kinase inhibition in the 6-furanylquinazoline series. *Bioorg. Med. Chem. Lett. 16*, 4686–4691.
22. Solowiej, J., Bergqvist, S., McTigue, M. A., Marrone, T., Quenzer, T., Cobbs, M., Ryan, K., Kania, R. S., Diehl, W., and Murray, B. W. (2009) Characterizing the effects of the juxtamembrane domain on vascular endothelial growth factor receptor-2 enzymatic activity, autophosphorylation, and inhibition by axitinib. *Biochemistry 48*, 7019–7031.
23. Choueiri, T. K. (2008) Axitinib, a novel anti-angiogenic drug with promising activity in various solid tumors. *Curr. Opin. Invest. Drugs 9*, 658–671.
24. Tummino, P. J., and Copeland, R. A. (2008) Residence time of receptor-ligand complexes and its effect on biological function. *Biochemistry 47*, 5481–5492.
25. Bull, H. G., Thornberry, N. A., Cordes, M. H., Patchett, A. A., and Cordes, E. H. (1985) Inhibition of rabbit lung angiotensin-converting enzyme by N alpha-[(S)-1-carboxy-3-phenylpropyl]L-alanyl-L-proline and N alpha-[(S)-1-carboxy-3-phenylpropyl]L-lysyl-L-proline. *J. Biol. Chem. 260*, 2952–2962.
26. Brandt, I., Joossens, J., Chen, X., Maes, M. B., Scharpe, S., De Meester, I., and Lambeir, A. M. (2005) Inhibition of dipeptidyl-peptidase IV catalyzed peptide truncation by Vildagliptin ((2S)-{[(3-hydroxyadamantan-1-yl)amino]acetyl}-pyrrolidine-2-carbonitrile. *Biochem. Pharmacol. 70*, 134–143.
27. Garvey, E. P., Schwartz, B., Gartland, M. J., Lang, S., Halsey, W., Sathe, G., Carter, H. L., III, and Weaver, K. L. (2009) Potent inhibitors of HIV-1 integrase display a two-step, slow-binding inhibition mechanism which is absent in a drug-resistant T66I/M154I mutant. *Biochemistry 48*, 1644–1653.
28. Swinney, D. C. (2004) Biochemical mechanisms of drug action: what does it take for success? *Nat. Rev. Drug Discov. 3*, 801–808.
29. Copeland, R. A., Williams, J. M., Giannaras, J., Nurnberg, S., Covington, M., Pinto, D., Pick, S., and Trzaskos, J. M. (1994) Mechanism of selective inhibition of the inducible isoform of prostaglandin G/H synthase. *Proc. Natl. Acad. Sci. U.S.A. 91*, 11202–11206.
30. Cheng, Y., and Prusoff, W. H. (1973) Relationship between the inhibition constant (K1) and the concentration of inhibitor which causes 50% inhibition (I50) of an enzymatic reaction. *Biochem. Pharmacol. 22*, 3099–3108.
31. Copeland, R. A. (2005) Evaluation of enzyme inhibitors in drug discovery. A guide for medicinal chemists and pharmacologists. *Methods Biochem. Anal. 46*, 1–265.
32. Morrison, J. F., and Walsh, C. T. (1988) The behavior and significance of slow-binding enzyme inhibitors. *Adv. Enzymol. Relat. Areas Mol. Biol. 61*, 201–301.
33. Manning, G., Whyte, D. B., Martinez, R., Hunter, T., and Sudarsanam, S. (2002) The protein kinase complement of the human genome. *Science 298*, 1912–1934.
34. Heerding, D. A., Rhodes, N., Leber, J. D., Clark, T. J., Keenan, R. M., Lafrance, L. V., Li, M., Safonov, I. G., Takata, D. T., Venslavsky, J. W., Yamashita, D. S., Choudhry, A. E., Copeland, R. A., Lai, Z., Schaber, M. D., Tummino, P. J., Strum, S. L., Wood, E. R.,

Duckett, D. R., Eberwein, D., Knick, V. B., Lansing, T. J., McConnell, R. T., Zhang, S., Minthorn, E. A., Concha, N. O., Warren, G. L., and Kumar, R. (2008) Identification of 4-(2-(4-amino-1,2,5-oxadiazol-3-yl)-1-ethyl-7-{[(3*S*)-3-piperidinylmethyl]oxy}-1*H*-imidazo[4,5-*c*]-pyridin-4-yl)-2-methyl-3-butyn-2-ol (GSK690693), a novel inhibitor of AKT kinase. *J. Med. Chem. 51*, 5663–5679.

35. Lohse, A., Hardlei, T., Jensen, A., Plesner, I. W., and Bols, M. (2000) Investigation of the slow inhibition of almond beta-glucosidase and yeast isomaltase by 1-azasugar inhibitors: evidence for the "direct binding" model. *Biochem. J. 349*, 211–215.
36. Rajagopalan, R., Misialek, S., Stevens, S. K., Myszka, D. G., Brandhuber, B. J., Ballard, J. A., Andrews, S. W., Seiwert, S. D., and Kossen, K. (2009) Inhibition and binding kinetics of the hepatitis C virus NS3 protease inhibitor ITMN-191 reveals tight binding and slow dissociative behavior. *Biochemistry 48*, 2559–2568.
37. Lebakken, C. S., Riddle, S. M., Singh, U., Frazee, W. J., Eliason, H. C., Gao, Y., Reichling, L. J., Marks, B. D., and Vogel, K. W. (2009) Development and applications of a broad-coverage, TR-FRET-based kinase binding assay platform. *J. Biomol. Screen. 14*, 924–935.
38. Neumann, L., Ritscher, A., Muller, G., and Hafenbradl, D. (2009) Fragment-based lead generation: identification of seed fragments by a highly efficient fragment screening technology. *J. Comput.-Aided Mol. Des.*
39. Shah, P. P., Myers, M. C., Beavers, M. P., Purvis, J. E., Jing, H., Grieser, H. J., Sharlow, E. R., Napper, A. D., Huryn, D. M., Cooperman, B. S., Smith, A. B., III, and Diamond, S. L. (2008) Kinetic characterization and molecular docking of a novel, potent, and selective slow-binding inhibitor of human cathepsin L. *Mol. Pharmacol. 74*, 34–41.
40. Wilhelm, S. M., Carter, C., Tang, L., Wilkie, D., McNabola, A., Rong, H., Chen, C., Zhang, X., Vincent, P., McHugh, M., Cao, Y., Shujath, J., Gawlak, S., Eveleigh, D., Rowley, B., Liu, L., Adnane, L., Lynch, M., Auclair, D., Taylor, I., Gedrich, R., Voznesensky, A., Riedl, B., Post, L. E., Bollag, G., and Trail, P. A. (2004) BAY 43-9006 exhibits broad spectrum oral antitumor activity and targets the RAF/MEK/ERK pathway and receptor tyrosine kinases involved in tumor progression and angiogenesis. *Cancer Res. 64*, 7099–7109.
41. Heinrich, M. C., Corless, C. L., Demetri, G. D., Blanke, C. D., von Mehren, M., Joensuu, H., McGreevey, L. S., Chen, C. J., Van den Abbeele, A. D., Druker, B. J., Kiese, B., Eisenberg, B., Roberts, P. J., Singer, S., Fletcher, C. D., Silberman, S., Dimitrijevic, S., and Fletcher, J. A. (2003) Kinase mutations and imatinib response in patients with metastatic gastrointestinal stromal tumor. *J. Clin. Oncol. 21*, 4342–4349.
42. Frost, M. J., Ferrao, P. T., Hughes, T. P., and Ashman, L. K. (2002) Juxtamembrane mutant V560GKit is more sensitive to Imatinib (STI571) compared with wild-type c-kit whereas the kinase domain mutant D816VKit is resistant. *Mol. Cancer Ther. 1*, 1115–1124.
43. Weisberg, E., Manley, P. W., Cowan-Jacob, S. W., Hochhaus, A., and Griffin, J. D. (2007) Second generation inhibitors of BCR-ABL for the treatment of imatinib-resistant chronic myeloid leukaemia. *Nat. Rev. Cancer 7*, 345–356.
44. Zhao, G., Peery, R. B., and Yingling, J. M. (2007) Characterization and development of a peptide substrate-based phosphate transfer assay for the human vascular endothelial growth factor receptor-2 tyrosine kinase. *Anal. Biochem. 360*, 196–206.
45. Atwell, S., Adams, J. M., Badger, J., Buchanan, M. D., Feil, I. K., Froning, K. J., Gao, X., Hendle, J., Keegan, K., Leon, B. C., Muller-Dieckmann, H. J., Nienaber, V. L., Noland, B. W., Post, K., Rajashankar, K. R., Ramos, A., Russell, M., Burley, S. K., and Buchanan, S. G. (2004) A novel mode of Gleevec binding is revealed by the structure of spleen tyrosine kinase. *J. Biol. Chem. 279*, 55827–55832.
46. Copeland, R. A., Pompliano, D. L., and Meek, T. D. (2006) Drug-target residence time and its implications for lead optimization. *Nat. Rev. Drug Discov. 5*, 730–739.
47. Lewandowicz, A., Tyler, P. C., Evans, G. B., Furneaux, R. H., and Schramm, V. L. (2003) Achieving the ultimate physiological goal in transition state analogue inhibitors for purine nucleoside phosphorylase. *J. Biol. Chem. 278*, 31465–31468.